

## Performance evaluation of a solar thermal and photovoltaic hybrid system powering a direct contact membrane distillation: TRNSYS simulation

Ahmed Remlaoui<sup>a,\*</sup>, Driss Nehari<sup>a</sup>, Mohammed Laissaoui<sup>b</sup>, Abdelfatah Marni Sandid<sup>a</sup>

<sup>a</sup>Smart Structure Laboratory, University Center of Ain-Temouchent, 46000 Ain-Temouchent, Algeria, email: donremlaoui@gmail.com (A. Remlaoui)

<sup>b</sup>Centre de Développement des Energies Renouvelables, CDER, B.P. 62. Route de l'Observatoire, 16040 Bouzaréah, Algiers, Algeria

Received 29 September 2019; Accepted 10 March 2020

---

### ABSTRACT

This paper investigates the integration of solar thermal and photovoltaic (PV) energy powering direct contact membrane desalination (DCMD) to produce clean water. The designed system includes a 2 m<sup>2</sup> flat plate collector (FPC) for thermal energy production, a stratified fluid storage tank with optional internal heater and heat exchangers with 0.3 m<sup>3</sup> of volume, DCMD modules for clean water production, and a PV panel with a maximum power of 55 W. The predicted performance of this system was analyzed and dynamically simulated using the TRNSYS (Transient System Simulation program) code. The DCMD unit was simulated and added to the software library. The DCMD unit and the thermal system were validated based on literature results. The dynamic simulation of this system was carried out in the region of Ain Témouchent (west of Algeria) throughout the year and focusing on 3 type days (24/01), (24/06), and (05/11). The obtained results show that the daily freshwater production by the system is around 59.34 L<sup>-1</sup> m<sup>2</sup> d<sup>-1</sup>, and that the temperature of the feed saltwater and the permeate flow through the DCMD system varies, respectively, from 60°C to 21°C and between 20°C and 34°C. In addition, the solar fraction (SF) reaches 0.41, 0.52, and 0.42 and the collector efficiency of FPC values reaches 52%, 64%, and 55% during the 3 selected days, respectively.

*Keywords:* Solar desalination; Direct contact membrane distillation; Flat plate collector; Photovoltaic panel; TRNSYS

---

### 1. Introduction

The world is suffering from water shortages and a growing need for access to safe water sources, especially for use as drinking water. As saltwater is abundant, interest in desalination processes is growing. Consequently, the construction of desalination plants is being developed on a large scale. The industrially created reverse osmosis (RO) technology for desalination requires large measures of energy [1].

On the other hand, several pilot plants for the desalination of sustainable energy sources have been installed, that

could use for example membrane distillation (hereafter MD). Almost all of them are specially designed for specific areas and use solar, wind, or geothermal energy to produce freshwater from seawater (SW) or brackish water (BW) assets.

MD is a hybrid process that combines both a thermal process and a membrane process. A hot aqueous feed solution is brought into contact with one side of a hydrophobic, microporous membrane. The driving force (also known as transmembrane vapor pressure difference) of the process is the partial pressure difference between the two sides of the membrane. It causes the supply side to evaporate and

---

\* Corresponding author.

transport the vapor through the dry pores of the hydrophobic membranes. Membranes with pore sizes ranging from 0.01 to 1 mm can be used in MD [2].

Membrane distillation stands out among the possibilities of exploiting solar energy for the most suitable desalination applications. Solar energy can be used to heat the feed solution and can also be connected to generate power to run the auxiliary hardware, normally supplied in a low-temperature range, that is, 70°C–90°C [3]. While most systems used for solar-driven MD are based on air-gap membrane distillation (AGMD), vacuum membrane distillation systems [4]. In addition to various configurations including direct contact membrane distillation (DCMD), permeate gap membrane distillation (PGMD), and sweeping gas membrane distillation.

Among these designs, DCMD presents the least difficult arrangement and is therefore probably the most appropriate for small-scale seawater desalination applications [5]. In the DCMD, the hot feed and the cold distillate are in direct contact with the membrane. Hot water is the seawater that has to be heated by a solar thermal energy system supplied by solar thermal collectors. PV (photovoltaic) provides the energy for auxiliary equipment such as pumps and valves.

Several seawater and brackish water desalination plants have been installed, which use the thermal energy supplied to MD via solar thermal collectors and solar photovoltaic panels for powering pumps and control systems. There are two different system configurations: (a) compact system (Gran Canaria, Spain [6,7]; Alexandria, Egypt [8]; and Irbid, Jordan [9]) and (b) two-loop system (Gran Canaria, Spain [7]; Aqaba, Jordan [10]; and Amarika, Namibia [11]).

A number of projects have been reported in the literature where MD technology is coupled with a hybrid solar thermal and PV energy systems (Gran Canaria, Spain [7]; Aqaba, Jordan [10]; and Amarika, Namibia [11]). These three multimodal two-loop units are used in AGMD [7] and PGMD [9,11] systems using solar thermal energy, which, respectively, consisted of 120, 40, and 168 m<sup>2</sup> spiral-wound membrane module and 186, 72, and 232 m<sup>2</sup> of solar thermal collector area. The outcome showed that these systems capacity was up to 1,400; 792; and 2,080 L d<sup>-1</sup>, respectively [12]. Zhani et al. [12] showed that the achieved heat consumption was 271, 200–300, and 171 kWh m<sup>-3</sup>, respectively. However, the majority of the works were carried out with PGMD or AGMD systems connected to the solar loop by heat exchanger outside the storage tank.

A major effort has been made to design efficient small-scale desalination units using numerical and experimental modeling [5,13–16]. TRNSYS (Transient System Simulation program) is an extensive software for transient simulation of energy systems, which is widely used by researchers and engineers to study and optimize solar systems. In this sense, Duong et al. [5] developed a model using TRNSYS to emulate the performance of an integrated DCMD–FPC (flat plate collector) system and demonstrated its validity on a small scale seawater desalination applications consisting of a 7.2 m<sup>2</sup> spiral-wound DCMD module and a 22.6 m<sup>2</sup> FPC capable of producing more than 140 kg of distillate per day.

On the other hand, Acevedo et al. [13] modeled and analyzed a small pilot plant providing electricity, sanitary hot water (SHW), and freshwater (FW). Power

(electricity) is extracted by coupling photovoltaic/thermal (PVT) collectors and a wind turbine (WT); SHW is produced from PVT and evacuated tube collectors (ETCs); FW is produced from PGMD and RO. The proposed baseline scenario produces up to 15,311 L y<sup>-1</sup> in the MD system and covers the electrical energy requirements up to 1,890 kWh. Vargas-Bautista et al. [14] studied a small-scale ethanol solar distillation system using ETCs and parabolic trough collectors (PTCs). For the thermal results, the authors showed by simulation that PTCs represents the best energy. Kumar and Martin [15] investigated experimentally and numerically various ways of coupling the membrane distillation (MD) process with solar domestic heaters for the co-production of domestic heat and pure water.

Mohan et al. [16] modeled and numerically analyzed a novel solar thermal polygeneration integrating membrane distillation (MD). The performance of the system was analyzed with three different solar collectors: FPC, ETC, and compound parabolic collector. The economic analysis conducted for the three collector configurations showed that the ETC has the lowest payback period of 9 y compared to the other two configurations.

Based on the above literature review and to the best of our knowledge, it appears that the thermal supply provided to the seawater that is necessary for the latter to reach the temperature required by the MD (50°C–80°C) [17,18] is mainly produced by the thermal collectors. In addition, these small desalination units lack an effective mechanism to quickly give the required temperature in a continuous direction. Furthermore, they avoid any excessive increase in temperature generated by these thermal collectors, especially during summer periods, which can cause significant deficiencies in the MD. Therefore, the design and study of a new small-scale solar desalination pilot, to be used with the FPC and the PV panels to produce the thermal supply needed for the saltwater, could be very interesting to ensure a continuous flow rate of saltwater with appropriate temperature and to analyze its feasibility.

Moreover, the previous literature review indicates that there is a lot of interest in the design of the different solar desalination systems using membrane distillation (MD) and solar energy. This is due to the need to create highly efficient and environmentally friendly designs.

In this direction, the paper aims to examine the best way to design an efficient solar desalination system. The analysis was conducted with a new type of component developed in TRNSYS related to the modeling of a DCMD and based on the analysis of a small hybrid DCMD solar desalination plant. The thermal and electric power required for the operation of the DCMD was provided respectively by a flat plate collector and a photovoltaic module. In this study, the solar fluid, saltwater temperatures, useful thermal energy, auxiliary heating rate, power at the maximum power point, Array power of PV array and power to load were discussed.

The reminder of the paper is organized as follows: section 2 describes the small-scale solar desalination system, while section 3 presents the simulations results and the performance of the thermal solar, photovoltaic and DCMD systems; finally, section 4 concludes the paper and provides several future perspectives.

**2. System description and modeling**

The studied system constitutes of a solar thermal flat plate collector and solar photovoltaic modules coupled to a DCMD. The system is designed to replace conventional sources with renewable sources to operate decentralized desalination systems. Fig. 1 presents a schematic diagram of the proposed system. Two main parts compose the considered system: the energy part, where the main elements are the FPC, stratified fluid storage tank with internal heat exchangers, pumps, PV connected with battery, and regulator/inverter, and DCMD module. The desalination part represented by a DCMD is described in detail in the following sections.

The first part of this work concerns the modeling of the DCMD by the creation of a new component in TRNSYS software, through the compilation of the Fortran subprogram in the last software. In the second part, the analysis of the proposed solar desalination system is presented.

The performance of the DCMD module is displayed by the outlet feed and permeate temperatures and the total mass flux transfer, in addition to comparisons between the simulated DCMD system and the literature data. It also shows the effects of the saltwater flow rate profile on the permeate flow. The system is modeled to operate during sunshine hours (08:00–18:00 h) in the region of Ain Témouchent, located in the west of Algeria.

Fig. 1 shows the schematic layout of the system considered for this study, it consists of three different subsystems.

**2.1. Solar thermal system**

Thermal energy is provided by an FPC solar collector and the solar energy is absorbed by the heat transfer fluid

(HTF). This heated fluid will supply a thermal storage tank. The HTF meets a coil heat exchanger to exchange its heat to the saltwater.

Fig. 1 shows a schematic outline of the solar desalination plant under investigation. The following parameters were considered: cold-water inlet temperature ( $T_1$ ), solar fluid temperature at inlet and outlet to the solar coil ( $T_5$  and  $T_2$ ), solar fluid temperature at inlet and outlet to the collector ( $T_3$  and  $T_4$ ), hot water supply temperature ( $T_6$ ), and the solar fluid and saltwater flow rates.

An FPC is a heat exchanger whose energy comes from the incident and diffuse solar radiation to working fluid HTF (water/glycol flow) [13]. Its thermal efficiency  $\eta_{coll}$  is given by the Hottel–Whillier–Bliss equation [14]:

$$\eta_{coll} = a_0 - a_1 \frac{(T_3 - T_{amb})}{I_T} - a_2 \frac{(T_3 - T_{amb})^2}{I_T} \tag{1}$$

where  $I_T$  the incident total solar radiation ( $\text{kJ h}^{-1} \text{m}^{-2}$ ),  $a_0$  is the intercept efficiency,  $a_1$  (efficiency slope), and  $a_2$  (efficiency curvature) are the first-order and the second-order coefficients in collector efficiency equation in ( $\text{kJ h}^{-1} \text{m}^{-2} \text{K}^{-1}$ ) and ( $\text{kJ h}^{-1} \text{m}^{-2} \text{K}^{-2}$ ) respectively;  $T_{amb}$  Ambient temperature ( $^{\circ}\text{C}$ ) and  $T_3$  is the inlet temperature of the fluid to the collector ( $^{\circ}\text{C}$ ).

The most effective method to determine the performance of the FPC is to calculate the useful thermal energy ( $Q_u$ ) transferred from the radiation to the HTF through the FPC in W [13]:

$$Q_u = \dot{m}_{HTF} C_{p,HTF} (T_4 - T_3) \tag{2}$$

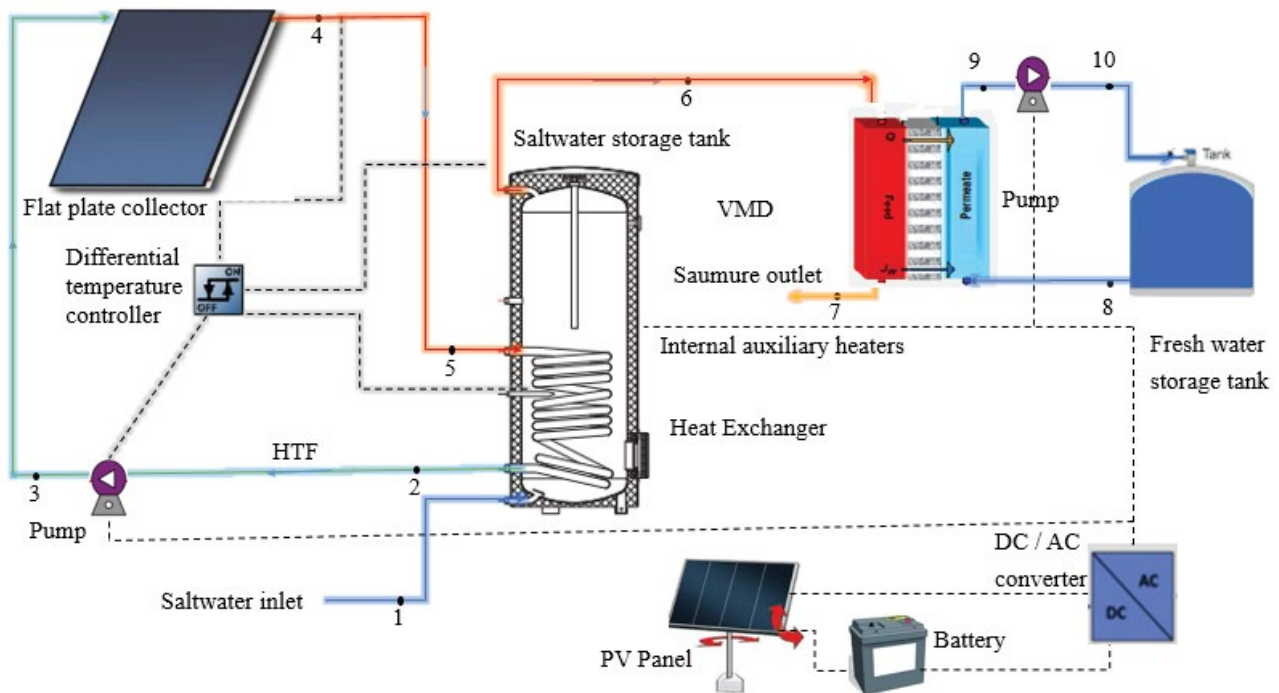


Fig. 1. Schematic layout of the distillation system assisted by solar energy.

where  $T_3$  and  $T_4$  are the temperatures of working fluid entering and leaving the FPC (K),  $\dot{m}_{\text{HTF}}$  is the solar fluid mass flow rate ( $\text{kg h}^{-1}$ ) and  $C_{p,\text{HTF}}$  is the specific heat of the fluid flowing through the solar collector array ( $\text{kJ kg}^{-1} \text{K}^{-1}$ );  $\eta_{\text{coll}}$  can be reformulated as:

$$\eta_{\text{coll}} = \frac{Q_u}{AI_T} \quad (3)$$

where  $A$  is the total area of the solar collector array ( $\text{m}^2$ ).

Eqs. (1)–(3) were used to calculate the steady-state collector output temperature at normal incidence as follows:

$$T_4 = T_3 + \frac{A}{\dot{m}_{\text{HTF}} C_{p,\text{HTF}}} \left( a_0 I_T + a_1 (T_3 - T_{\text{amb}}) - a_2 (T_3 - T_{\text{amb}})^2 \right) \quad (4)$$

After studying the most important component of the thermal system, the FPC, the storage tank specialized in fluid storage is the next step. It consists of an internal heat exchanger to absorb the useful energy of the HTF and internal heaters to add energy as required. The energy balance can then be expressed with the following equation [19]:

$$M_i C_p \frac{dT}{dt} = Q_{\text{env}} + Q_{\text{cond}} + Q_{\text{hx}} + Q_{\text{aux}} + Q_{\text{inject}} + Q_{\text{flue}} \quad (5)$$

where  $Q_{\text{env}}$  is the flow of energy exchanged by convection between the storage tank and the ambient air (W),  $Q_{\text{cond}}$  is the energy flow exchanged by conduction between two layers (W),  $Q_{\text{inject}}$  is the energy flow linked to the injection of cold or hot water into the balloon (W),  $Q_{\text{flue}}$  is the flow of convective energy exchanged with a possible chimney (W),  $Q_{\text{hx}}$  is the energy flow produced by the heat exchanger (W),  $Q_{\text{aux}}$  is the flow of energy produced by an auxiliary heater (W),  $C_p$  is the specific heat of the fluid contained in the storage tank (saltwater) ( $\text{kJ kg}^{-1} \text{K}^{-1}$ ),  $M_i$  is the mass of saltwater in node  $i$  (kg).

The use of a variable speed pump is a great advantage to improve the system performance based on the radiation level hitting the collector. The outlet temperature of the pump ( $T_3$ ) is calculated as follows:

$$T_3 = T_2 + \frac{\dot{Q}_{\text{HTF}}}{\dot{m}_{\text{HTF}}} \quad (6)$$

where  $\dot{Q}_{\text{HTF}}$  is the energy transferred from the pump motor to the fluid stream passing through the pump ( $\text{kJ h}^{-1}$ ) and calculated as:

$$\dot{Q}_{\text{HTF}} = \dot{P}_{\text{shaft}} (1 - \eta_{\text{pumping}}) + (\dot{P} - \dot{P}_{\text{shaft}}) f \quad (7)$$

where the pumping process requires shaft power  $\dot{P}_{\text{shaft}}$  ( $\text{kJ h}^{-1}$ ),  $\dot{P}$  is the power drawn by the pump at the current time ( $\text{kJ h}^{-1}$ ),  $f$  is a fraction of the pump motor inefficiencies and  $\eta_{\text{pumping}}$  is fluid pumping efficiency.

The solar fraction (SF) is one of the most important performance coefficients of the thermal system. It is defined as the ratio between the energy provided by the solar collector ( $Q_u$ ) and the total amount of solar energy needed to

operate the desalination system (the power was added to the tank by the auxiliary heater  $Q_{\text{aux}}$ ), and is given by [20]:

$$\text{SF} = \frac{Q_u}{Q_u + Q_{\text{aux}}} \quad (8)$$

## 2.2. Solar PV system

The electrical system contains photovoltaic modules, a battery bank, and an inverter. The system is designed to be standalone, that is, it is used to supply electricity for the pump and auxiliary heater in the storage tank (after converting the DC to AC). The batteries chemically store direct current electrical energy for later use during periods of cloudy weather.

The power output ( $P_{\text{PV}}$ ) from the PV array, depending on the irradiance and the temperature, is expressed as [21]:

$$P_{\text{PV}} = P_{\text{PV,STC}} f_{\text{STC}} \frac{G}{G_{\text{STC}}} \left[ 1 + \alpha_p (T_c - T_{c,\text{STC}}) \right] \quad (9)$$

where  $P_{\text{PV,STC}}$  is the output power under standard test conditions (STC), and STC (standard test conditions: Air Mass = 1.5,  $G_{\text{STC}} = 1,000 \text{ W m}^{-2}$ ,  $T_{c,\text{STC}} = 25^\circ\text{C}$ ),  $f_{\text{STC}}$  is the PV derating factor,  $G$  is the total radiation incident on PV array,  $G_{\text{STC}}$  is the incident radiation at STC,  $\alpha_p$  is the temperature coefficient of the power,  $T_c$  is the PV module temperature, and  $T_{c,\text{STC}}$  is the PV module temperature under STC [21].

After, the total  $P_{\text{PV}}$  of PV panel is determined; the battery capacity in Ampere-hour (Ah) can be calculated using Eq. (10) as follows:

$$C = \frac{P_{\text{load}} \times N_j}{n_b \times P_d \times \text{pr}} \quad (10)$$

where  $P_{\text{load}}$  is the required energy during the day ( $\text{Wh d}^{-1}$ ),  $N_j$  is the number of autonomy days (1 d with a minimum solar irradiation rate) required,  $P_d$  is the depth of discharge,  $n_b$  is the battery efficiency, and pr is the losses.

## 2.3. DCMD system

In the DCMD, the hot feed solution (saltwater) enters the module at temperature  $T_6$  and mass flow rate  $m_{f,\text{in}}$ . The gaseous fraction of this solution (distillate  $m_d$ ) permeates through the membrane and is mixed with the cooling solution at the permeate side with temperature  $T_9$  and mass flow rate  $m_{p,\text{in}}$ . The rest of the feed solution is the concentrate which exits the module at a temperature  $T_7$  and mass flow rate  $m_c$  at the feed side, as for the permeate side, the outlet permeates solution with temperature  $T_8$  and mass flow rate  $m_{p,\text{out}}$  as shown in Fig. 1.

A simple model was used, it depends on the mean global mass and heat transfer coefficients which are respectively  $C_{\text{global}}$  ( $\text{L h}^{-1} \text{m}^{-2} \text{pa}^{-1}$ ) and  $U$  ( $\text{J h}^{-1} \text{m}^{-2} \text{K}^{-1}$ ) and experimentally obtained by Zhang [18] at the same stream velocity  $V$  ( $\text{m s}^{-1}$ ). This model estimates the flux of a large sheet membrane and the temperature profile for a co-current case flow. The membrane with a pore size of  $0.5 \mu\text{m}$  and a scrim support layer

was used. The adjustment equations of the mean global mass and heat transfer coefficients can be expressed as [17,18]:

$$U = -5,248V^2 + 4,735.7V - 36.036 \quad (11)$$

$$C_{\text{global}} = -0.004V^2 + 0.0053V - 0.0001 \quad (12)$$

In the DCMD, the mass flux ( $\text{L m}^{-2} \text{h}^{-1}$ ) can be expressed as follows:

$$J_w = C_{\text{global}} \Delta P \quad (13)$$

where  $\Delta P$  is the vapor pressure difference between the feed and permeate (Pa).

The following assumptions in developing the model were made [17]:

- The insulated thermal unit can ignore the heat exchange with the environment through the module wall;
- The latent heat of evaporation and condensation does not change with concentration, as stated by Lunnon [22];
- The values of  $C_{\text{global}}$  and  $U$  do not change for a given membrane and a given flow rate;
- There is no gradual temperature change across the membrane perpendicular to the flow direction;
- In the mass transfer balancing equation, the mass of the permeate can be neglected.

Using these assumptions, the general mass flux form can be expressed as follows:

$$J_w = C_{\text{global}} (P_{\text{bf}} - P_{\text{bp}}) \quad (14)$$

where  $P_{\text{bf}}$  and  $P_{\text{bp}}$  are the partial pressures of the water on the hot and cold feed membrane surfaces (Pa), respectively.

These pressures are estimated using the Antoine equation [5]:

$$P = \exp\left(23.1964 - \frac{3,816.44}{T - 46.13}\right) \quad (15)$$

where  $T$  is the temperature (K) of the feed and distillate at the membrane surface.

Fig. 2 shows the heat transfer of a co-current DCMD in three regions.

- The heat transfer in the hot side ( $Q_f$ ) can be described as follows [23]:

$$Q_f = C_{p,f} \dot{m}_f (T_{f,i+1} - T_{f,i}) \quad (16)$$

- The heat flux ( $Q$ ) through the membrane ( $Q_m$ ) is a combination of the conduction heat and the latent heat. In a small element it can be described as [5]:

$$Q_m = U(T_{f,i} - T_{p,i})dA + J_w \Delta H_v dA \quad (17)$$

- The heat transfer in the cold side ( $Q_p$ ) can be described as follows [23]:

$$Q_p = C_{p,p} \dot{m}_p (T_{p,i} - T_{p,i+1}) \quad (18)$$

In Eqs. (15)–(18),  $\dot{m}_f$  and  $\dot{m}_p$  are the mass flow rates of the feed and permeate streams ( $\text{kg s}^{-1}$ ),  $C_{p,f}$  and  $C_{p,p}$  are the feed and permeate specific heat capacity ( $\text{kJ kg}^{-1} \text{K}^{-1}$ ),  $\Delta H_v$  is the latent heat of water vaporization ( $\text{J L}^{-1}$ ),  $T_{(f,p),i}$  and  $T_{(f,p),i+1}$  are the temperatures at the  $i$ th and  $(i + 1)$ th points,  $dA = w dx$  where,  $A$  is the membrane area ( $\text{m}^2$ ),  $w$  is the membrane width (m).

According to Eqs. (16) and (17), the feed temperature change is calculated as:

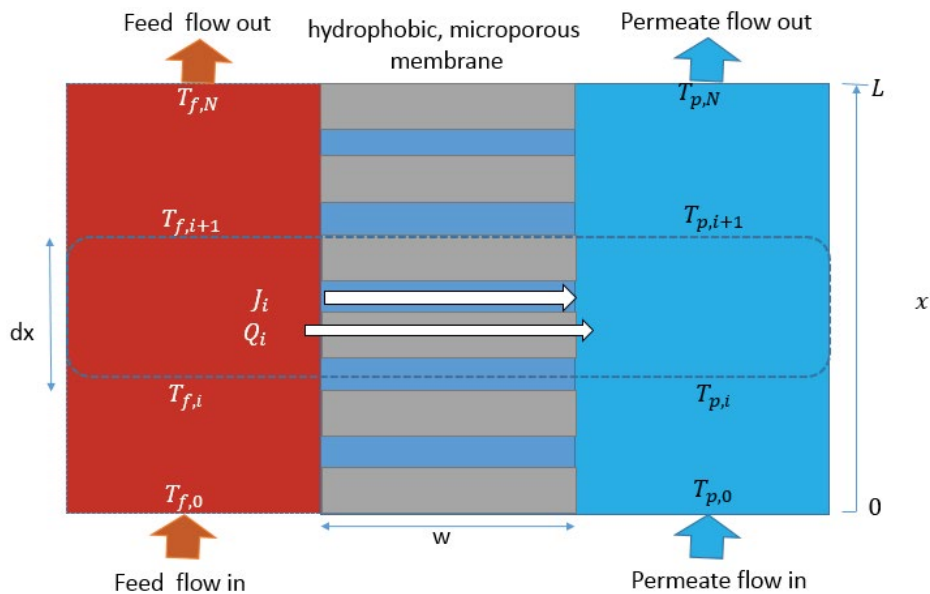


Fig. 2. Heat and mass transfer from a co-current DCMD to a flat sheet module.

$$\Delta T_{f,i} = - \frac{[U(T_{f,i} - T_{p,i}) + J_w \Delta H_v] w dx}{C_{p,f} \dot{m}_{f,i}} \quad (19)$$

According to Eqs. (17) and (18), the permeate temperature change is calculated as:

$$\Delta T_{p,i} = \frac{[U(T_{f,i} - T_{p,i}) + J_w \Delta H_v] w dx}{C_{p,p} \dot{m}_{p,i}} \quad (20)$$

According to assumption 3, the feed and permeate temperatures at the  $(i + 1)$ th station can be calculated by:

$$T_{f,i+1} = T_{f,i} - \Delta T_{f,i} \quad (21)$$

$$T_{p,i+1} = T_{p,i} - \left( \frac{m_f}{m_p} \right) \Delta T_{f,i} \quad (22)$$

Because  $C_{\text{global}}$  and  $U$  are assumed to be constants (assumption 3). The mass and heat flux transfer at the  $(i + 1)$ th station can be calculated as:

$$J_{i+1} = C_{\text{global}} (P_{f,i+1} - P_{p,i+1}) \quad (23)$$

$$Q_{i+1} = U (T_{f,i+1} - T_{p,i+1}) \quad (24)$$

Therefore, the total mass and heat flux transfer can be described as:

$$J = \frac{\sum_{i=0}^N J_i W \Delta x}{A} \quad (25)$$

$$Q = \frac{\sum_{i=0}^N Q_i W \Delta x}{A} \quad (26)$$

Fig. 3 shows the algorithms calculations of the DCMD procedure for the co-current. The computation starts at the fluid inlet ( $x = 0$ ) and ends at the fluid outlet ( $x = L$ ) of the DCMD module, where  $L$  is the membrane length (m).

#### 2.4. TRNSYS simulation of solar-DCMD system

TRNSYS version 17 software was used to design and study the performance of an integrated solar thermal and photovoltaic DCMD system. Fig. 4 represents the main component of the solar thermal system. It includes: a FPC (Type 1b); a variable speed water pump (Type 110); a Type 60d stratified fluid storage tank with optional internal heaters and optional internal heat exchangers with 1 inlet and 1 outlet; a Type 2b differential temperature controller; Type 14 forcing functions, hot water demand profile (Type 14b), hot water demand temperature (Type 14e) and immersion heater control signals (Type 14h); Type 31 pipes ducts.

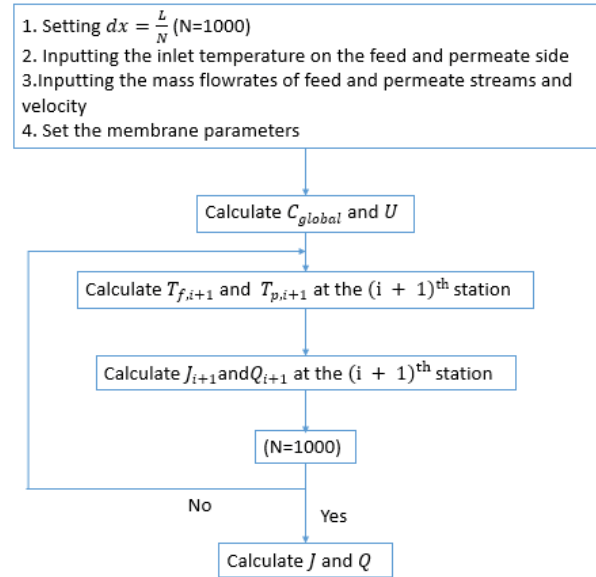


Fig. 3. Flow diagram for the DCMD model for the calculation of the heat and mass flow of the co-current flow.

The TRNSYS standard component includes the electrical power systems used in this work: photovoltaic panels TYPE94a; electrical storage TYPE47c; regulator/inverter TYPE48b.

Other components include: unit conversion routine Type 57, Type 65c online plotters with files, TYPE109-TMY2 weather data reading and processing and TYPE24 integrator.

A newly developed component called TYPE 223, was added to the standard library and dedicated to the modeling of a DCMD unit. This component was written by FORTRAN language. Table 1 presents the different parameter values of the DCMD model.

In this work, the saltwater flowrate profiles illustrated in Fig. 5 are the same as those used by Ayompe et al. [24]. Tables 2–4 summarize the parameters of the system used in the TRNSYS [24].

The solar fluid mass flow rate was introduced into the thermal system using Eq. (27) (equivalent in the TRNSYS system assembly diagram), which changes linearly with solar radiation, the coefficients  $a$  and  $b$  are 0.0100 and  $-2.1394$ , respectively [24]:

$$\dot{m}_{st} = a I_t + b \quad (27)$$

The parameters for PV panels (Siemens SM55) with a maximum rated power of 55 W and a maximum power point voltage of 17.4 V are given in Table 5 obtained from Chaker et al. [25] and used in the TRNSYS model with Type 94a.

### 3. Results and discussion

In this study, the plant used was validated and simulated throughout the year in the town of Ain Témouchent in ALGERIA. To simplify the representation of the results obtained, 3 d were chosen, namely (24/01), (24/06), and (05/11).

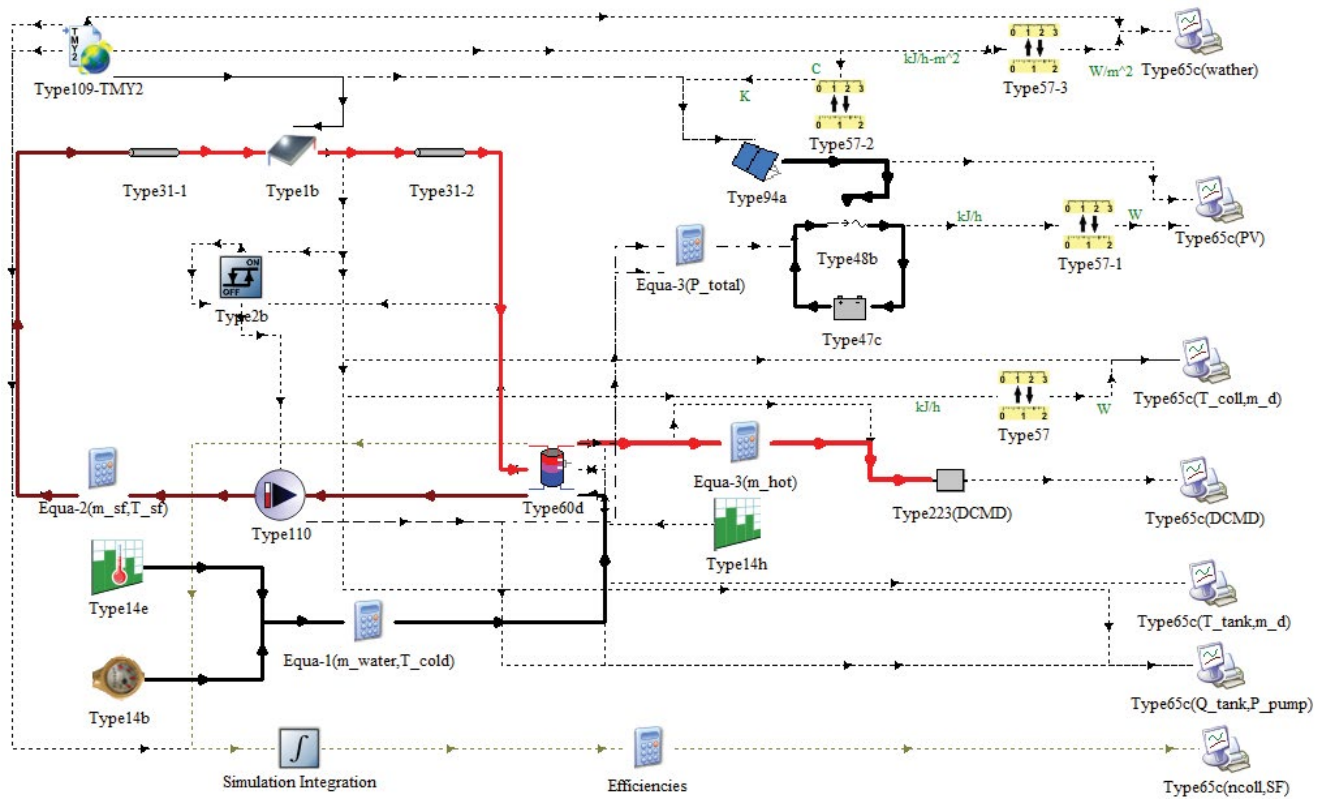


Fig. 4. System assembly diagram of the solar desalination system in TRNSYS simulation studio.

Table 1  
Parameters for the DCMD model [17]

Parameters	Value
Membrane material	PTFE
Membrane length, m	0.145
Pore size, $\mu\text{m}$	1
Contact angle, $^\circ$	126
Membrane area, m	0.0136
Membrane width, m	0.1
Specific heat of freshwater, $\text{J kg}^{-1} \text{K}^{-1}$	4,190
Specific heat of feed water, $\text{J kg}^{-1} \text{K}^{-1}$	4,190
Feed water speed, $\text{m s}^{-1}$	0.4
Salinity $g_{\text{NaCl}} L_{\text{water}}^{-1}$	10

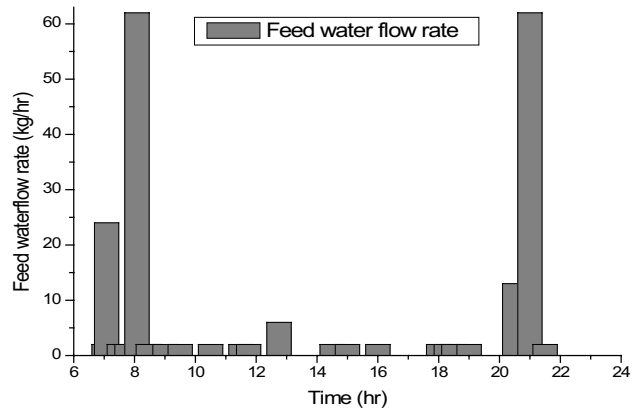


Fig. 5. Feedwater load variation during the day [24].

### 3.1. Model validation of the DCMD model and thermal system

Several simulations were carried out to verify the DCMD model with different membrane lengths with a pore size of  $0.5 \mu\text{m}$  and a scrim support layer. The Perspex module was used for co-current configurations. A comparison was made with the work by Zhang [17,18] (Fig. 6).

Fig. 6a shows the comparison between the experimental results of Zhang's study [18] and our numerical results derived from the DCMD model using the following characteristics: flow velocity of  $0.4 \text{ m s}^{-1}$ , the cold inlet temperature of  $20^\circ\text{C}$  and the hot inlet temperature of  $60^\circ\text{C}$ . The permeate

flux predicted by the current model is in good agreement with the flux result of Zhang [18].

In addition, Fig. 6b shows the temperature distributions of the feed and permeate sides as well as of the membrane module in co-current flow mode under the following conditions: an inlet permeate temperature of  $20^\circ\text{C}$ , an inlet feed temperature of  $60^\circ\text{C}$ ; fluid flow velocity of  $0.4 \text{ m s}^{-1}$  and a total membrane length of  $0.145 \text{ m}$ . The result indicates a good agreement between the present numerical model and the numerical model [17].

The effects of feed temperature and feed velocity on permeate flow were studied by Zhang et al. [17]. The optimal

parameters are  $0.4 \text{ m s}^{-1}$  and  $60^\circ\text{C}$ . The feed velocity of  $0.4 \text{ m s}^{-1}$  achieves the most permeation and the increase in feed rate requires an increase in heating and therefore high energy consumption for heating and pumping. The same conclusion is reached for an increase in feed temperature.

Fig. 7 illustrates the comparison between present-modeled results (a) collector outlet temperature for FPC and (b) heat collected by FPC and heat delivered to load and experimental results obtained by Ayompe et al. [24]. Ayompe et al. [24] modeled and simulated the performance of a solar water heating systems used in temperate climates of Ireland. The used collectors were two FPCs (K420-EM2L)

consisting of a total area of  $4 \text{ m}^2$  and a hot water cylinder (model HM 300L D/coil U44332). The present thermal system was compared to the experimental system according to weather conditions prevalent in Ireland for a summer day (02/06/2009) and showed good consistency and concordant results (Figs. 7a and b).

### 3.2. Meteorological data

Three representative days: summer day (24/06), autumn day (05/11), and winter day (24/01) were used to predict the performance of the solar thermo-photovoltaic system powering the DCMD module over 1 y in Ain Témouchent,

Table 2  
Hot water cylinder (Type 60d) parameters

Parameter	Value
Tank volume ( $\text{m}^3$ )	0.3
Tank height (m)	1.68
Height of flow inlet 1 (m)	0.1
Height of flow outlet 1 (m)	1.6
Fluid specific heat ( $\text{kJ kg}^{-1} \text{K}^{-1}$ )	4.19
Fluid density ( $\text{kg m}^{-3}$ )	1,000
Tank loss coefficient ( $\text{W m}^{-2} \text{K}^{-1}$ )	0.3
Fluid thermal conductivity ( $\text{kJ h}^{-1} \text{m}^{-1} \text{K}^{-1}$ )	1.4
Boiling temperature ( $^\circ\text{C}$ )	100
Height of 1st auxiliary heater (m)	1
Height of 1st thermostat (m)	1.5
Set point temperature for element 1 ( $^\circ\text{C}$ )	60
Dead band for heating element 1 ( $^\circ\text{C}$ )	5
Maximum heating rate of element 1 ( $\text{kJ h}^{-1}$ )	9,900
Fraction of glycol	0.4
Heat exchanger inside diameter (m)	0.016
Heat exchanger outside diameter (m)	0.02
Heat exchanger fin diameter (m)	0.02
Total surface area of heat exchanger ( $\text{m}^2$ )	2
Heat exchanger length (m)	32
Heat exchanger wall conductivity ( $\text{kJ h}^{-1} \text{m}^{-1} \text{K}^{-1}$ )	1.8
Heat exchanger material conductivity ( $\text{kJ h}^{-1} \text{m}^{-1} \text{K}^{-1}$ )	1.8
Height of heat exchanger inlet (m)	0.9
Height of heat exchanger outlet (m)	0.1

Table 5  
Photovoltaic panel (Type94a) parameters [25]

Parameter	Value
Module short-circuit current at reference conditions (A)	3.45
Module open-circuit voltage at reference conditions (V)	21.7
Module voltage at max power point and reference conditions (V)	17.4
Module current at max power point and reference conditions (A)	3.5
Number of modules in series	3
Number of modules in parallel	6
Module temperature at NOCT ( $^\circ\text{C}$ )	45
Module area ( $\text{m}^2$ )	0.82

Table 3  
Flat plate collector (Type 73) parameters [24]

Parameter	Value
Number in series	1
Collector absorber area ( $\text{m}^2$ )	2
Fluid specific heat ( $\text{kJ kg}^{-1} \text{K}^{-1}$ )	3.708
Tested flow rate ( $\text{kg h}^{-1} \text{m}^{-2}$ )	80
Intercept efficiency	0.776
First order efficiency coefficient ( $\text{kJ h}^{-1} \text{m}^{-2} \text{K}^{-1}$ )	14.22
Second order efficiency coefficient ( $\text{kJ h}^{-1} \text{m}^{-2} \text{K}^{-2}$ )	0.0594
Maximum flow rate ( $\text{kg h}^{-1}$ )	212
Collector slope ( $^\circ$ )	53
Absorber plate emittance	0.7
Absorbance of absorber plate	0.8
Number of covers	1
Index of refraction of cover	1.526
Extinction coefficient thickness product	0.28

Table 4  
Variable speed pump (Type 110) parameters [24]

Parameter	Value
Rated flow rate ( $\text{kg h}^{-1}$ )	212
Fluid specific heat ( $\text{kJ kg}^{-1} \text{K}^{-1}$ )	3.708
Rated power ( $\text{kJ h}^{-1}$ )	226.8

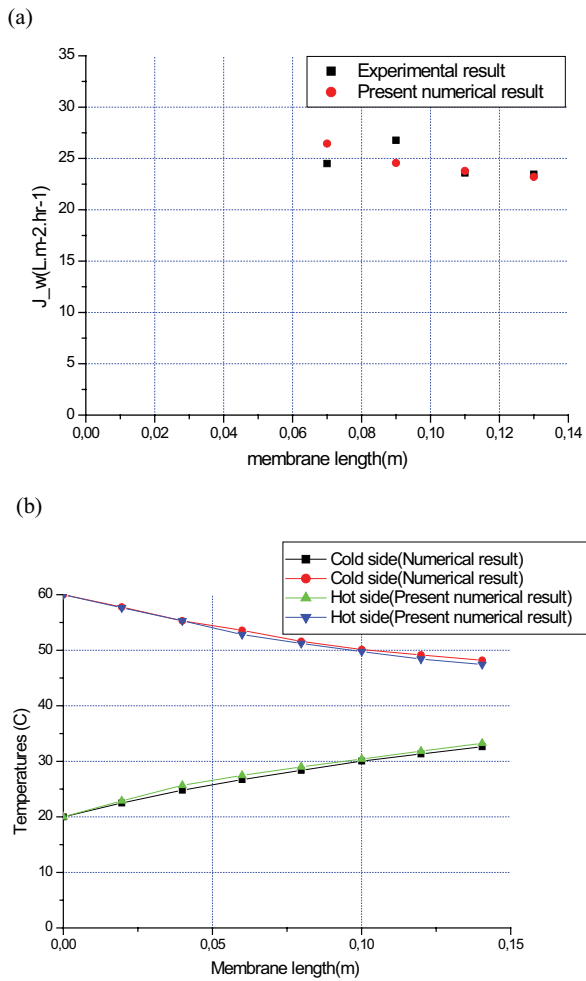


Fig. 6. Validation of the present numerical model at ( $T_{p,o} = 20^\circ\text{C}$ ,  $T_{f,o} = 60^\circ\text{C}$ ,  $V = 0.4 \text{ m s}^{-1}$ ). (a) Comparison of permeate flux between experimental result of Zhang [18] and the present numerical result and (b) comparison of temperatures distributions of the feed and the permeate sides between the numerical result of Zhang et al. [17] and the present numerical result.

Algeria. Figs. 8a–c show the wind speed, ambient air temperature and solar radiation, respectively.

During these selected days, the peak of total solar radiation were 687.88, 518.08, and 551.98  $\text{W m}^{-2}$ , respectively. The highest ambient temperatures were 27.82°C, 17.57°C, and 11.025°C, respectively. On the other hand, for wind speed, the peaks for these days are 2.95, 5.45, and 1.8  $\text{m s}^{-1}$ , respectively.

### 3.3. Thermal system performance

Fig. 9 displays: (a) collector outlet temperature  $T_4$  and (b) useful thermal energy  $Q_u$  for the FPC system over three significant days. The results of the simulation indicate that the collector outlet temperature is limited between 7.35°C and 43.75°C on a winter day (24/01). On a summer day (24/06), the collector outlet temperature is ranged between 18.19°C and 55.74°C, whereas in on a autumn day (05/11)

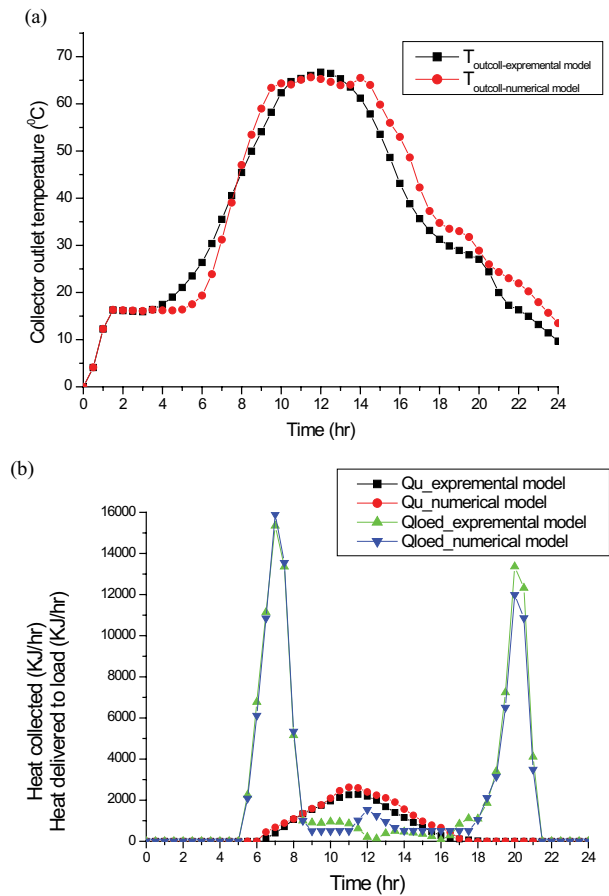


Fig. 7. Validation of the numerical model with the experimental model of Ayompe et al. [24]. (a) Collector outlet temperature and (b) heat collected by the FPC and heat delivered to load.

the collector outlet temperature reaches the maximum value of 45.41°C and the minimum value of 11.96°C (Fig. 9a).

Fig. 9b shows that the useful energy gain from the FPC field reaches a maximum of 540.24, 774.69, and 537.18 W respectively, during the tested days. This change is due to a difference in the meteorological data (solar radiation) during the 3 d of the seasons (as shown in Fig. 8).

The collector reaches its maximum collector outlet temperature and useful thermal energy when the solar radiation reaches the highest value. The summer day gives the highest values of outlet temperature and useful thermal energy compared to the other selected days.

With regard to the performance parameters of the thermal system, the collector efficiency is analyzed for the 3 d as shown in Fig. 10. This parameter is achieved: 52%, 64%, and 55% during the operating hours for the 3 d, respectively.

Fig. 11 shows (a) the solar fluid outlet tank temperature ( $T_2$ ), (b) hot water outlet temperature ( $T_6$ ), and (c) the energy delivered by the auxiliary heater ( $Q_{aux}$ ) throughout the day. It can be noted that:

- The temperature of the seawater exiting the storage tank ( $T_6$ ) shows stability from the beginning of the day till 8 am with a value of 60°C, then decreases to 52.91°C, 52.84°C, and 52.91°C during the 3 tested days respectively. This

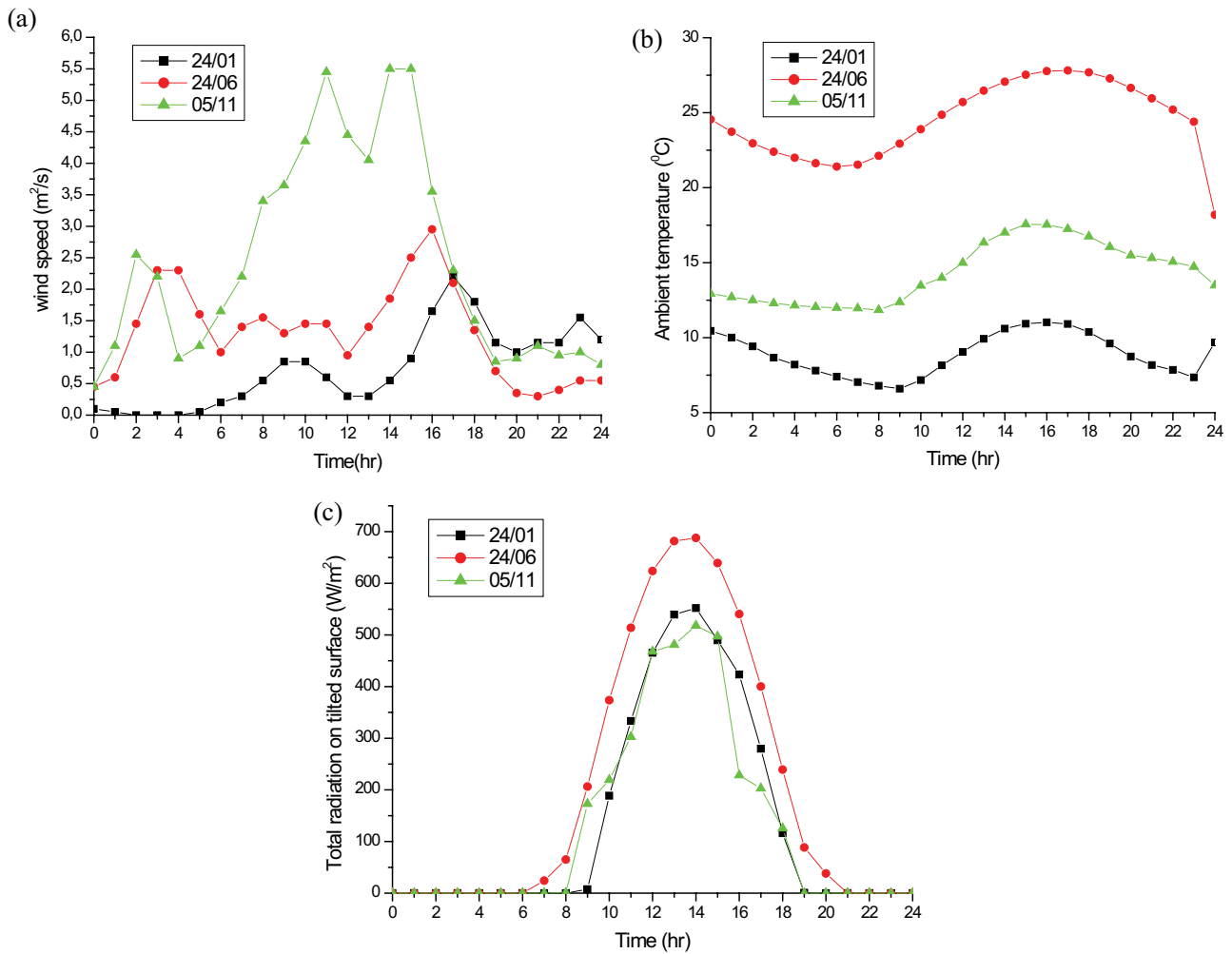


Fig. 8. Variations weather data in (a) wind speed, (b) ambient air temperature, and (c) solar radiation over 3 d in Ain Témouchent, Algeria.

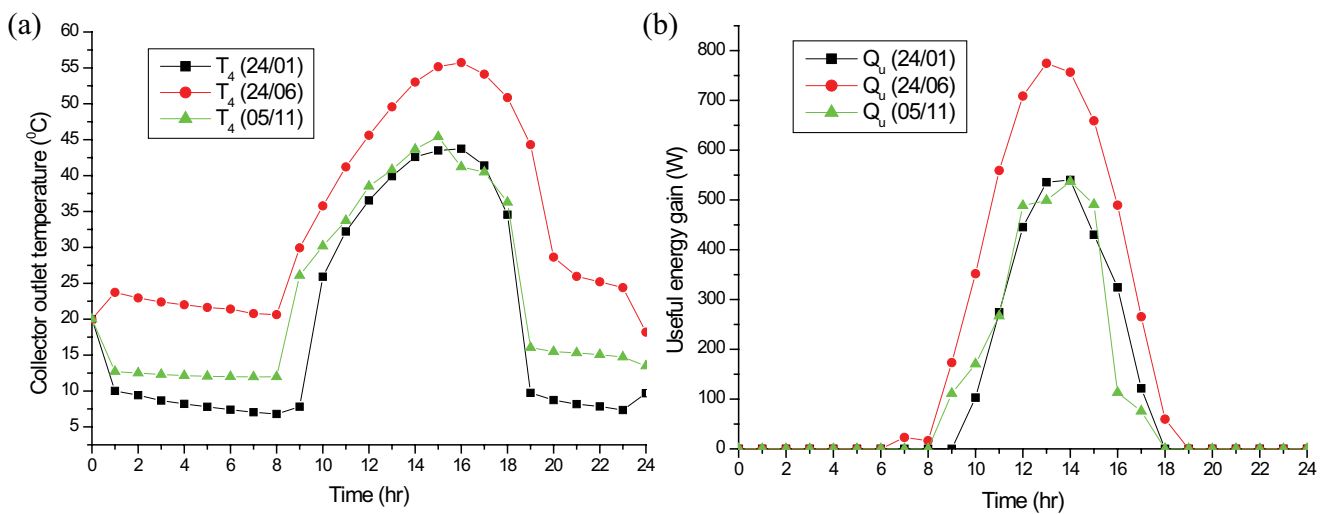


Fig. 9. Variations of FPC parameters over 3 d in (a) FPC outlet temperature and (b) the useful thermal energy  $Q_u$ .

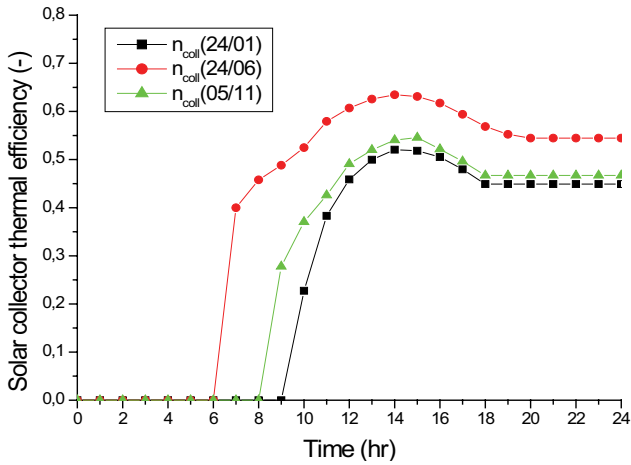


Fig. 10. Solar collector thermal efficiency  $\eta_{coll}$  during 3 d.

is due to the use of the auxiliary heater linked to the thermostat to reach the required temperature (setpoint temperature is 60°C and dead band for heating is 5°C).

- The temperature of the solar fluid exiting the specified internal heat exchanger ( $T_2$ ) shows the height up to 40.49°C, 51.90°C, and 41.20°C, respectively during the chosen days. The HTF temperature remains high at the outlet of the tank, due to its recycling in the several times of the solar loop and also due to an increase in the temperature of lower layers of the tank.
- The auxiliary heating consumes the highest values of 9,900 kJ h<sup>-1</sup> from 6 am to 9 am, the same for the 3 tested days, and 1,830.35; 4,647.18; and 3,777.89 kJ h<sup>-1</sup> in the hourly range between 6 pm and 9 pm for the 3 tested days, respectively. This means that the high value of the solar radiation leads to minimize the intervention of the auxiliary heating to raise the temperature of the brackish water up to 60°C.

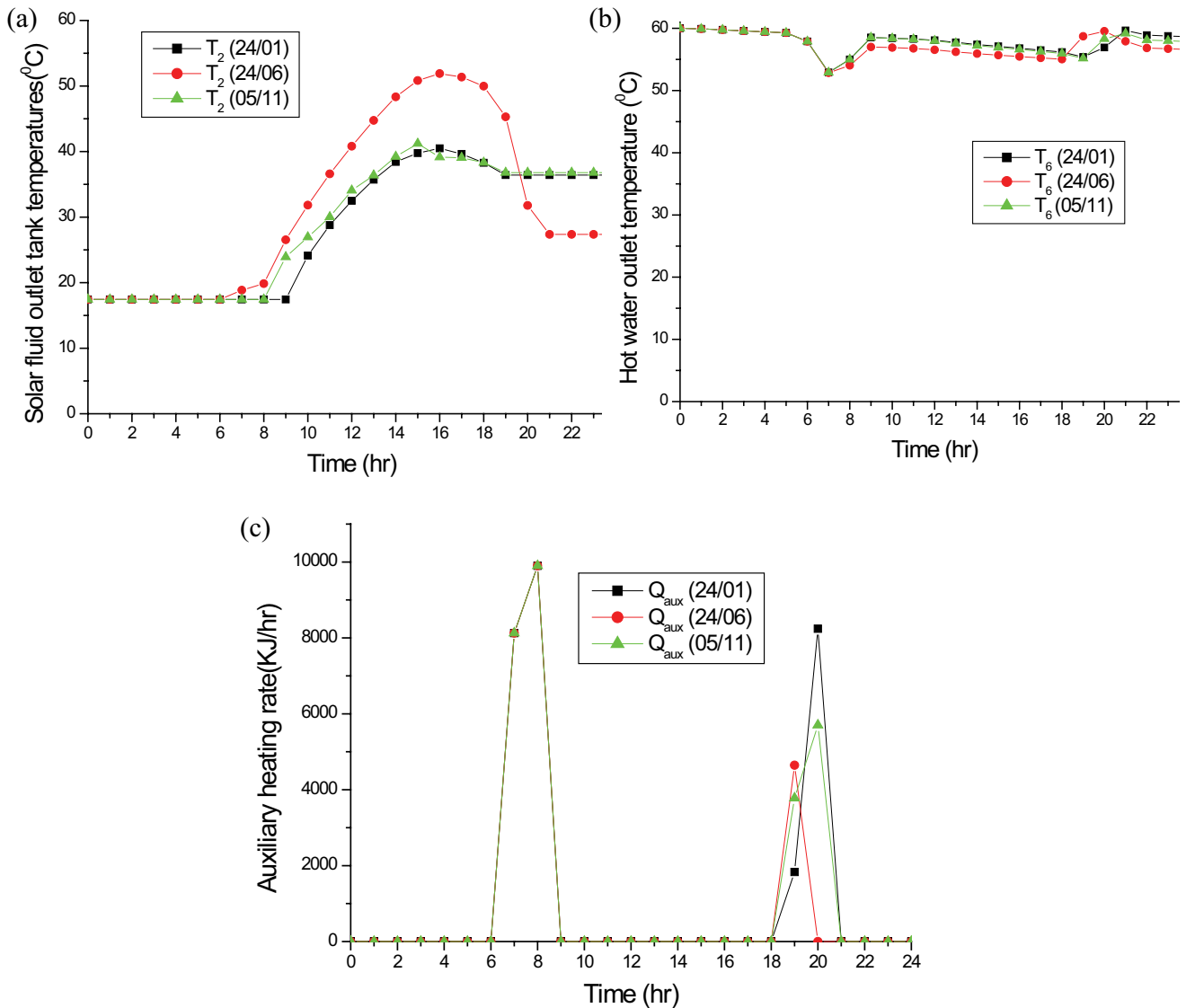


Fig. 11. Variations of solar tank parameters over 3 d in (a) solar fluid outlet tank temperature  $T_2$  and (b) hot water outlet temperature  $T_6$  and (c) auxiliary heating rate  $Q_{aux}$ .

As it is well-known in our plant, the PV supplies the pump with electricity and auxiliary heat is added to the seawater through the PV temperature control system. Therefore, the PV system is an auxiliary system and the thermal system is the basic system. The same conclusion is explained by the SF value (Fig. 12). The solar saving fraction gets a value close to 1, this is due to the fact that the energy for heating saltwater is supplied only by solar thermal [Eq. (8)].

### 3.4. Performance of PV system

This section describes the power at maximum power point ( $P_{mpp}$ ) and array power ( $P_{array}$ ), (b) power from PV array ( $P_{from PV array}$ ) and power to load ( $P_{to load}$ ) (Fig. 13a).

On a summer day, the power predicted at MPP shows a maximum value up to 3,375.97 W. The other 2 test days in the fall and winter of the season show excellent results up to 2,577.60 and 2,470.52 W, respectively. The predicted nominal array power for 2 d (autumn and winter) is 298.90 and 304.49 W, which is half the expected value for the summer test day is 445.36 W (Fig. 13a).

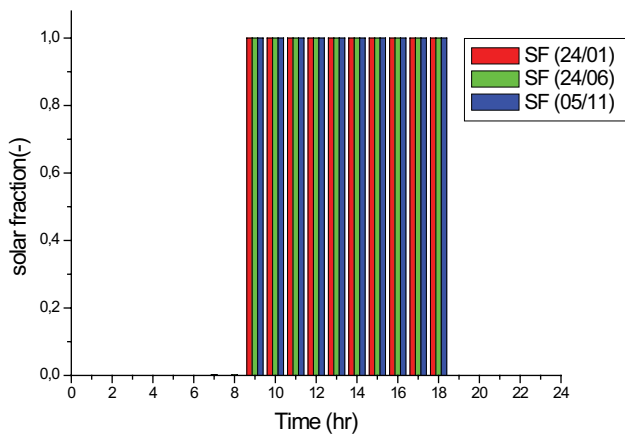


Fig. 12. Solar fraction (SF) over 3 d.

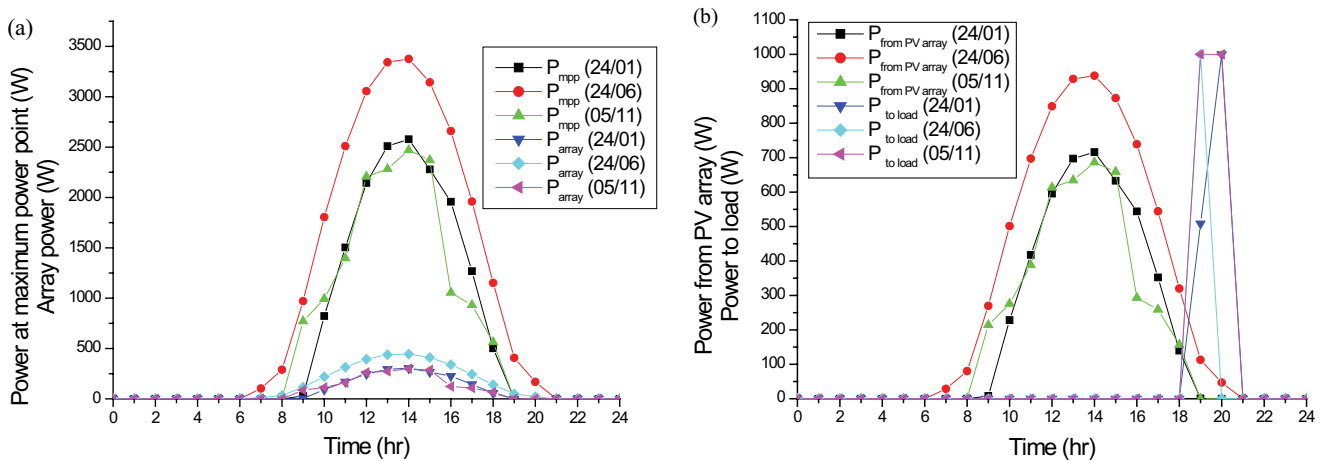


Fig. 13. Variation of the PV system performance over 3 d in (a) power at maximum power point and array power of PV array and (b) power from PV array and power to load.

Fig. 13b shows the power from PV array and power to load. The power from PV array reaches a maximum of 716, 937.78, and 686.25 W on the test days respectively and the change overs from 7 am to 8 pm. In this time frame, it can be observed that there is no power to load. Subsequently, it reaches high results up 1,000 W for the 3 test days.

### 3.5. Performance of the DCMD module

Fig. 14 illustrates (a) the Outlet feed and permeate temperatures  $T_f$ ,  $T_s$  and (b) the total mass flux transfer  $J$  for DCMD system for each hour during the 3 d. At the feed side, the salt-water outlet temperature ( $T_f$ ) fluctuates between 60°C and 21°C. Thus, on the permeate side, freshwater outlet temperature ( $T_s$ ) varies from 20°C to 3°C.

The permeate flow of the DCMD system is influenced by the temperature, masse flow rate, and concentration of the feed water for a given membrane module. Fig. 14b shows the permeate flux variation. The distillate production per membrane area reaches its highest value of 11.09 L h<sup>-1</sup> m<sup>-2</sup>. However, the value of daily distillate production of the present study is 59.34 L m<sup>-2</sup> d. Distillate production per membrane area reaches its highest value compared with plants with other technologies membrane, as shown in Table 6.

Fig. 14b also shows that the permeate flow rate values are lower from 6 to 21 h. This is due to a lower feed flow rate, although there is a good radiation. The last part of this section describes an improvement in the feed flow rate and note its effect on the permeate flow.

Fig. 15 shows the effect of saltwater flowrate profile on the permeate flow. The first profile illustrates the use of saltwater between 6 am and 8 am and between 6 pm and 9 pm, the second profile shows the use of saltwater between 8 and 18 h (Fig. 15a). Fig. 15b clarifies an increase in the value of permeate between 8 and 18 h for the second profile compared to the first one. This is due to the use of thermal energy. The value of distilled water for the second profile is higher compared to the first profile during the day (10 h) (Table 7).

Table 6  
Comparison between the simulated DCMD system and the data from the literature

Configurations	Simulated data from the present study	Data in the for similar study			
		Duong et al. [5]	Banat et al. [9]	Fath et al. [8]	Koschikowski et al. [26]
	Flat-sheet DCMD module	Spiral-wound DCMD module	PGMD (permeate gap membrane distillation)	PGMD	AGMD
Membrane area (m <sup>2</sup> )	0.0136	7.2	10	–	8
Thermal collector area (m <sup>2</sup> )	3.95	22.6	5.73	5.73	5.9
Daily distillate production/membrane area (kg m <sup>-2</sup> d <sup>-1</sup> )	59.34	19.72	<12	–	10.12

4. Conclusion

This study aimed to evaluate and analyze the performance of solar thermal and photovoltaic systems coupled with DCMD unit. A solar thermal (FPC) and PV DCMD system for the production of freshwater from brackish water was designed and tested using TRNSYS version 17 software.

The study case was adapted for the region of Ain Témouchent (Algeria) throughout the year and on 3 type days: winter day (24/01), summer day (24/06), and autumn day (05/11). As TRNSYS has not yet been designed to model desalination processes, a new type was created to achieve the complete simulation. The obtained results show that the predicted permeate flux data closely matches the measured permeate flux data.

The total solar radiation peaks are 551.98, 687.88, and 518.08 W m<sup>-2</sup> on these days respectively and the highest ambient temperatures are 11.025°C, 27.82°C, and 17.57°C, respectively. The collector outlet temperature is between 7.35°C and 43.75°C for winter day (21/01). In summer day (21/06) is between 18.19°C and 55.74°C, whereas in the autumn day (21/11), the collector outlet temperature reaches

Table 7  
Comparison between the solar and DCMD system using two saltwater flowrate profile at the same time (thermal energy only)

Time (10 h)	Total mass flux transfer J for DCMD system		
	Profile 1	Profile 2	Profit
24/01	4.47	17.80	13.33
24/06	4.28	19.78	15.50
05/11	4.46	17.98	13.52

the maximum value of 45.41°C and the minimum value of 11.96°C. The useful energy gain from the FPC field reaches a maximum of 540.24, 774.69, and 537.18 W and the collector efficiency of FPC reaches: 52%, 64%, and 55% during the operating hours for the 3 d, respectively.

The auxiliary heating consumed the same highest value of 9,900 kJ h<sup>-1</sup> from 6 am to 9 am, for the 3 test days and 1,830.35; 4,647.18; and 3,777.89 kJ h<sup>-1</sup> in the hourly range between 6 pm and 9 pm for 3 test days, respectively.

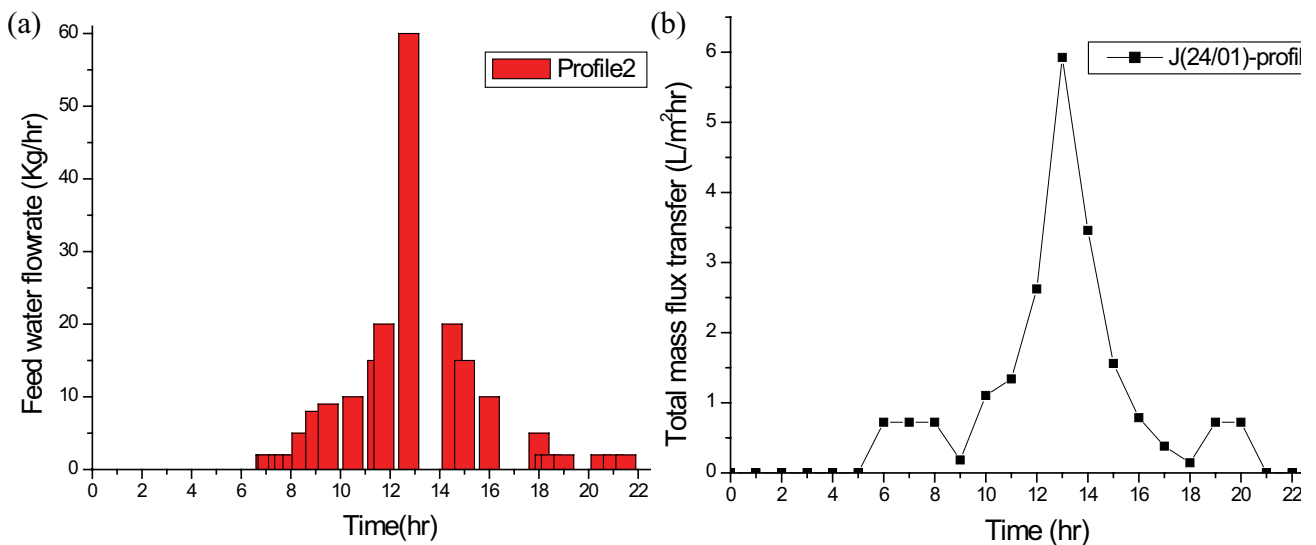


Fig. 15. Effects of saltwater flowrate profile on the permeate flow in variation of (a) feedwater flowrate and (b) total mass flux transfer J for DCMD system over day (24/01).

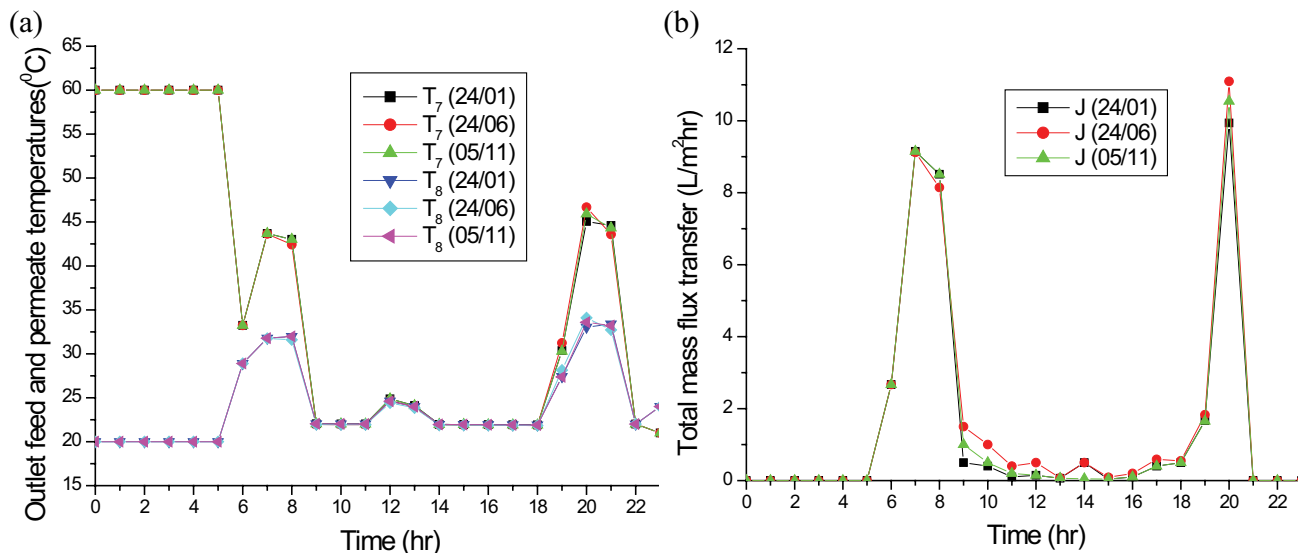


Fig. 14. Variation of permeate temperatures and flux in (a) outlet feed and permeate temperatures  $T_7$ ,  $T_8$  and (b) total mass flux transfer  $J$  for DCMD system.

The highest solar fraction is one in the first 6 h of the 3 d, after that, it ranges between 0.16 and 0.39 from 7 am to 8 pm. In the last hours of the 3 test days, the solar fraction is 0.41 and 0.42 in winter and autumn days, respectively, whereas in summer the solar fraction is 0.52.

The predicted power at the MPP for PV system shows a maximum value up to 3,375.97W. The two remaining test days of autumn and winter showed good results up to 2,577.60 and 2,470.52 W, respectively. The saltwater outlet temperature for DCMD system fluctuates between 60°C and 21°C and freshwater outlet temperature varies from 20°C to 34°C. The daily distillate production for this study is 59.34 L m<sup>-2</sup> d.

The results obtained are part of a series of works in the field of solar desalination. Consequently, several future perspectives can be noted: (i) applying this system in different coastal (Mediterranean seawater) or desert (Brackish water) areas, (ii) reusing the concentrated water or recovering the lost heat to heat the saltwater before entering the thermal system, and (iii) optimizing the system on the technical-economic level to evaluate the updated cost of fresh water.

### Acknowledgments

The authors acknowledge the financial support of the FNRS/DT/DGRSDT within the framework of ERANETMED3 (Project ERANETMED3-166 EXTRASEA) of the Directorate General for Scientific Research and Technological Development.

### Symbols

$T$	— Temperature, K
$Q_u$	— Useful thermal energy, W
$C_p$	— Specific heat of fluid, kJ kg <sup>-1</sup> K
$A$	— Total area of the solar collector array or membrane area, m <sup>2</sup>
$C_{\text{global}}$	— Mean global mass coefficient, L h <sup>-1</sup> m <sup>-2</sup> pa
$U$	— Heat transfer coefficient, J h <sup>-1</sup> m <sup>-2</sup> K
$V$	— Stream velocity, m s <sup>-1</sup>

$J_w$	— Mass flux, L m <sup>-2</sup> h
$\Delta P$	— Vapour pressure difference between the feed and permeate, Pa
$P$	— Partial pressures of the water, Pa
$Q$	— Energy, W
$M_i$	— Mass of saltwater in node $i$ , kg
$C$	— Battery capacity, Ah
$\Delta H_v$	— Latent heat of water vaporization, J L <sup>-1</sup>
$\Delta T$	— temperature change
$W$	— Membrane width, m
$\dot{m}$	— Mass flow rate, Kg s <sup>-1</sup>
$a$ and $b$	— Coefficients of Solar fluid mass flow rate
$P_{\text{load}}$	— Required energy during the day, Wh d <sup>-1</sup>
$P_d$	— Depth of discharge
$n_b$	— Battery efficiency
$f_{\text{STC}}$	— PV derating factor,
$f$	— Fraction of pump motor inefficiencies
$N_j$	— Number of autonomy days, d
$U_b$	— Nominal voltage of the batteries, v
$P_{\text{PV}}$	— Power output of PV array, W
$G$	— Total radiation incident on PV array, W m <sup>-2</sup>
$\dot{P}$	— Power, kJ h <sup>-1</sup>
$I_T$	— Incident total solar radiation, kJ h <sup>-1</sup> m <sup>2</sup>
$a_0$	— Intercept efficiency
$a_1$	— Efficiency slope, kJ h m <sup>-2</sup> K
$a_2$	— Efficiency curvature, kJ h <sup>-1</sup> m <sup>-2</sup> K <sup>2</sup>
SF	— Solar fraction

### Greek

$p$	— Temperature coefficient of the power, W K <sup>-1</sup>
$\eta$	— Efficiency, %

### Subscripts

1	— Cold-water inlet position
5	— Solar fluid at inlet to the solar coil position
2	— Solar fluid at outlet to the solar coil position

3	—	Solar fluid at inlet to the collector position
4	—	Solar fluid at outlet to the collector position
6	—	Hot water supply position
7	—	Outlet concentrate position
8	—	Outlet permeate position
9	—	Inlet permeate position
amb	—	Ambient
c	—	PV module
Bf	—	Hot feed membrane surface
bp	—	Cold permeate membrane surface
<i>i</i> th	—	the <i>i</i> <sup>th</sup> points
( <i>i</i> + 1)th	—	the ( <i>i</i> + 1) <sup>th</sup> points
sf	—	Solar fluid
<i>f</i>	—	Feed
<i>p</i>	—	Permeate
<i>C</i>	—	Concentrate
<i>D</i>	—	Distillate
In	—	Inlet
Out	—	Outlet
STC	—	Standard test conditions
shaft	—	Pumping process requires shaft
coll	—	Thermal collector
pumping	—	pumping the fluid
env	—	Exchanged by convection between the storage tank and the ambient air
cond	—	Exchanged by conduction between two layers
inject	—	Injection of cold or hot water into the tank
flue	—	Convective energy exchanged with a possible chimney
hx	—	Heat exchanger
aux	—	Auxiliary heater

## References

- [1] M. Laïssaoui, P. Palenzuela, M.A.S. Eldean, D. Nehari, D.C.A. Padilla, Techno-economic analysis of a stand-alone solar desalination plant at variable load conditions, *Appl. Therm. Eng.*, 133 (2018) 659–670.
- [2] P. Pal, A.K. Manna, Removal of arsenic from contaminated groundwater by solar-driven membrane distillation using three different commercial membranes, *Water Res.*, 44 (2010) 5750–5760.
- [3] A. Cipollina, E. Tzen, V. Subiela, M. Papapetrou, J. Koschikowski, R. Schwantes, M. Wiegghaus, G. Zaragoza, Renewable energy desalination: performance analysis and operating data of existing RES-desalination plants, *Desal. Water Treat.*, 55 (2016) 1–21.
- [4] A. Ali, R.A. Tufa, F. Macedonio, E. Curcio, E. Drioli, Membrane technology in renewable-energy-driven desalination, *Renewable Sustainable Energy Rev.*, 81 (2018) 1–21.
- [5] H.C. Duong, L. Xia, Z. Ma, P. Cooper, W. Ela, L.D. Nghiem, Assessing the performance of solar thermal driven membrane distillation for seawater desalination by computer simulation, *J. Membr. Sci.*, 542 (2017) 133–142.
- [6] R.G. Raluy, R. Schwantes, V.J. Subiela, B. Peñate, G. Melián, J.R. Betancort, Operational experience of a solar membrane distillation demonstration plant in Pozo Izquierdo-Gran Canaria Island (Spain), *Desalination*, 290 (2012) 1–13.
- [7] J. Koschikowski, M. Wiegghaus, M. Rommel, V.S. Ortin, B.P. Suarez, J.R.B. Rodríguez, Experimental investigations on solar driven stand-alone membrane distillation systems for remote areas, *Desalination*, 248 (2009) 125–131.
- [8] H.E.S. Fath, S.M. Elsherbiny, A.A. Hassan, M. Rommel, M. Wiegghaus, J. Koschikowski, M. Vatansver, PV and thermally driven small-scale stand-alone solar desalination systems with very low maintenance needs, *Desalination*, 225 (2008) 58–69.
- [9] F. Banat, N. Jwaied, M. Rommel, J. Koschikowski, M. Wiegghaus, Desalination by a “compact SMADES” autonomous solarpowered membrane distillation unit, *Desalination*, 217 (2007) 29–37.
- [10] F. Banat, N. Jwaied, M. Rommel, J. Koschikowski, M. Wiegghaus, Performance evaluation of the “large SMADES” autonomous desalination solar-driven membrane distillation plant in Aqaba, Jordan, *Desalination*, 217 (2007) 17–28.
- [11] R. Schwantes, A. Cipollina, F. Gross, J. Koschikowski, D. Pfeifle, M. Rolletschek, V. Subiela, Membrane distillation: solar and waste heat driven demonstration plants for desalination, *Desalination*, 323 (2013) 93–106.
- [12] K. Zhani, K. Zarzoum, H. Ben Bacha, J. Koschikowski, D. Pfeifle, Autonomous solar powered membrane distillation systems: state of the art, *Desal. Water Treat.*, 57 (2015) 1–14.
- [13] L. Acevedo, J. Uche, A. Del Almo, F. Círez, S. Usón, A. Martínez, I. Guedea, Dynamic simulation of a trigeneration scheme for domestic purposes based on hybrid techniques, *Energies*, 9 (2016) 1–25.
- [14] J.P. Vargas-Bautista, A.J. García-Cuéllar, S.L. Pérez-García, C.I. Rivera-Solorio, Transient simulation of a solar heating system for a small-scale ethanol-water distillation plant: thermal, environmental and economic performance, *Energy Convers. Manage.*, 134 (2017) 347–360.
- [15] N.T.U. Kumar, A.R. Martín, Co-production performance evaluation of a novel solar combi system for simultaneous pure water and hot water supply in urban households of UAE, *Energies*, 10 (2017) 1–22.
- [16] G. Mohan, U. Kumar, M. Kumar, A. Martin, A novel solar thermal polygeneration system for sustainable production of cooling, clean water and domestic hot water in United Arab Emirates: dynamic simulation and economic evaluation, *Appl. Energy*, 167 (2015) 173–188.
- [17] J. Zhang, J.-D. Li, S. Gray, Researching and modelling the dependence of MD flux on membrane dimension for scale-up purpose, *Desal. Water Treat.*, 31 (2011) 144–150.
- [18] J. Zhang, Theoretical and Experimental Investigation of Membrane Distillation, Ph.D. Thesis, Institute for Sustainability and Innovation, School of Engineering and Science, Victoria University, 2011. Available at: <http://vuir.vu.edu.au/16101/>.
- [19] B.J. Newton, Modeling of Solar Storage Tanks, M.S. Thesis, University of Wisconsin–Madison, Dissertations Academic Mechanical Engineering, University of Wisconsin–Madison, College of Engineering, 1995.
- [20] A. Hobbi, K. Siddiqui, Optimal design of a forced circulation solar water heating system for a residential unit in cold climate using TRNSYS, *Solar Energy*, 83 (2009) 700–714.
- [21] C. Ghenai, A. Merabet, T. Salameh, E.C. Pigem, Grid-tied and stand-alone hybrid solar power system for desalination plant, *Desalination*, 435 (2018) 172–180.
- [22] R.G. Lunnon, The latent heat of evaporation of aqueous salt solutions, *Proc. Phys. Soc. London*, 25 (2002) 180–191.
- [23] B.B. Ashoor, S. Mansour, A. Giwa, V. Dufour, S.W. Hasan, Principles and applications of direct contact membrane distillation (DCMD): a comprehensive review, *Desalination*, 398 (2016) 222–246.
- [24] L.M. Ayompe, A. Duffy, S.J. McCormack, M. Conlon, Validated TRNSYS model for forced circulation solar water heating systems with flat plate and heat pipe evacuated tube collectors, *Appl. Therm. Eng.*, 31 (2011) 1536–1542.
- [25] R. Chaker, H. Mhiri, H. Dhauouadi, P. Bournot, A TRNSYS dynamic simulation model for photovoltaic system powering a reverse osmosis desalination unit with solar energy, *Int. J. Chem. Reactor Eng.*, 8 (2010) 1542–6580.
- [26] J. Koschikowski, M. Wiegghaus, M. Rommel, Solar thermal-driven desalination plants based on membrane distillation, *Desalination*, 156 (2003) 295–304.